CAE v1.1—A Code for the Magnetic Field Due to Arbitrary Electromagnets

Divyang R. Prajapati[1] and Gattu Ramesh Babu[2]

[1]Department of Physics, St. Xavier's College, Ahmedabad 380009, India
[2]Institute for Plasma Research, Gandhinagar 382428, India

The Code for the magnetic field due to Arbitrary Electromagnets (CAE) v1.1 is a feature-rich version of CAE v1.0 code to simulate the magnetic fields generated by arbitrary electromagnetic systems. The code calculates the magnetic field due to straight and circular segments of zero thickness or rectangular cross section and cylindrical wire. The magnetic field calculations use a combination of analytical and numerical integration methods based on the Biot–Savart law. The design philosophy of CAE is to reduce the complexities while generating the inputs, and provide the visuals of the given inputs as 3-D plots of the electromagnets and magnetic field components as outputs in the Excel format. The code is successfully verified with the standard examples and the EFFI implementation on BETA, ADITYA-U, and SST-1 tokamaks.

***Index Terms*— Code, electromagnets, magnetic field, tokamak.**

I. Introduction

THE Institute for Plasma Research (IPR) is engaged in magnetic fusion research and has two tokamaks, ADITYA-U [1], [2] and SST-1 [3], and is also involved in the next level tokamaks viz. SST-2, spheromak, DEMO, and ITER. The tokamaks, stellarators and many other plasma devices use electromagnets to generate the magnetic fields of desired shapes and values for confining the charged particles. Several codes, viz. EFFI [4], ABCXYZ [5], MAFCO [6] were developed earlier to simulate such magnetic fields. However, the generation of the input files for these codes is a tedious and challenging task [7]. Visualization of these coils based on the input files is also not available. The contours and plots generation based on the output data are not inbuilt and require other programs. Hence, we require an easy and user-friendly customizable code for the modifications of existing tokamaks and the design of future machines with electromagnets.

A *C*ode for the magnetic field due to *A*rbitrary *E*lectromagnets (henceforth referred as CAE) has an easy input file format, generation of visuals of the electromagnets, and so on that makes it a better choice over the existing codes. Python 3.6 was chosen as the programming language to keep this code compatible with both the operating systems, Windows 10 and Ubuntu 18.04, without any modifications. The code has two important features: design stage—the zero cross-sectional filaments are used in designing the shapes of the magnetic fields and development stage—the conductors with rectangular/circular cross-sectional area can be used in electromagnet design, postfabrication, and at installation stages. CAE v1.0 [8] was restructured with most of the modules as functions, improved with two input files (with logical options viz. permeability, generation of visuals, current direction) to CAE v1.1. The results are also verified with EFFI.

Also, this version has a module to calculate the magnetic field due to a cylindrical wire and another module, CAEB v1.0 to generate the symmetrical coils data based on a single coil. The code also has a feature to generate contours.

Analytical derivation of the formulae for the magnetic field due to current in arbitrary conductor geometries is not possible. Hence, the methods used for the calculations in this code are based on a combination of both analytical and numerical integration (Simpson's rule) of the Biot–Savart law for a volume distribution of the current.

Section II details the analytical formulae for the magnetic field due to the chosen electromagnet shapes and configurations. Section III details about the methodology followed to calculate the magnetic fields of arbitrarily positioned electromagnets with the formulae derived as in Section II. Section IV explains the flow of the CAE code. Section V is about the code outputs. Section VI presents the verification of the code. The code results related to BETA, ADITYA-U, and SST-1 systems are presented in Section VII followed by conclusion in Section VIII.

II. Analytical Formulae for Magnetic Field Due to Electromagnet Elements

All the electromagnets in this code are of straight and circular arcs only as any shaped electromagnet can be approximated as a combination of straight and different circular arcs of different radii. The user generates the dimensional data related to the straight and circular arcs of the electromagnets from the CAD drawings, a prerequisite to this code.

The Biot–Savart law with a constant current I is

$$\vec{B}(P) = \frac{\mu_0 I}{4\pi}\vec{H} = \frac{\mu_0 I}{4\pi}\int_A^B \frac{d\vec{l'} \times (\vec{R} - \vec{R'})}{|\vec{R} - \vec{R'}|^3} \tag{1}$$

where μ_0 is the permeability of free space. A and B are the opposite ends of the conductor. $\vec{R}$ and $\vec{R'}$ are the space and

Manuscript received May 10, 2019; accepted July 13, 2019. *(Divyang R. Prajapati and Gattu Ramesh Babu contributed equally to this work.)* Corresponding author: G. R. Babu (e-mail: gattu@ipr.res.in).

Color versions of one or more of the figures in this article are available online at http://ieeexplore.ieee.org.

Digital Object Identifier 10.1109/TMAG.2019.2932287

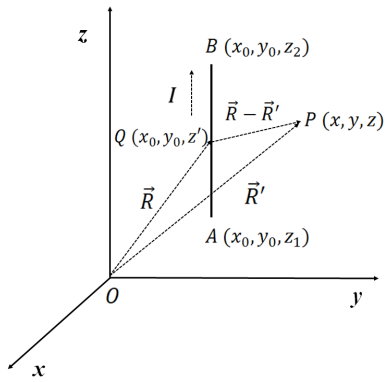

Fig. 1. Configuration of a straight filament.

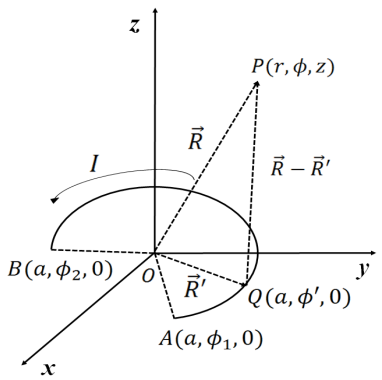

Fig. 2. Configuration of a circular filament.

source points' position vectors respectively. $d\vec{l}'$ is the vector differential element in the direction of the current.

For the geometries with finite volume, the Biot–Savart law involving the constant current density term J is

$$\vec{B}(P) = \frac{\mu_0 J}{4\pi}\vec{H} = \frac{\mu_0 J}{4\pi}\int_A^B ds' \frac{d\vec{l}' \times (\vec{R} - \vec{R}')}{|\vec{R} - \vec{R}'|^3} \tag{2}$$

where ds' is the differential element of the cross-sectional area orthogonal to $d\vec{l}'$.

A. Straight Filament of Zero Thickness

Fig. 1 shows the orientation of the straight filament for which we derive the formula.

The straight filament is parallel to the Z-axis and has a length of $(z_2 - z_1)$. The space and source points are $P(x, y, z)$ and $Q(x_0, y_0, z')$, respectively, with $d\vec{l}' = dz'\hat{k}$ and $z_1 \le z' \le z_2$ [9]. For this configuration, the cross product $d\vec{l}' \times (\vec{R} - \vec{R}')$ of (1) is

$$dz'\hat{k} \times [(x - x_0)\hat{i} + (y - y_0)\hat{j} + (z - z')\hat{k}] = [v\hat{i} - u\hat{j}]\, dw \tag{3}$$

where $u = x - x_0$, $v = y - y_0$, and $w = z - z'$.

$\vec{H}$ in (1) for this case becomes

$$\vec{H} = \int_{w_1}^{w_2} \frac{dw}{(a^2 + w^2)^{\frac{3}{2}}} \begin{cases} v, & \text{(x-component)} \\ -u, & \text{(y-component)} \\ 0, & \text{(z-component).} \end{cases} \tag{4}$$

On integrating and substituting the limits

$$\vec{H} = \frac{1}{a^2}\left(\frac{w_2}{\sqrt{a^2 + w_2^2}} - \frac{w_1}{\sqrt{a^2 + w_1^2}}\right) \begin{cases} v \\ -u \\ 0 \end{cases} \tag{5}$$

with $a^2 = u^2 + v^2$, $w_2 = z - z_2$ and $w_1 = z - z_1$.

B. Circular Filament of Zero Thickness

Fig. 2 shows the orientation of the circular filament for which we derive the formula.

The circular filament is in the XY plane, which has a radius a and an azimuthal length, $(\phi_2 - \phi_1)$. The space and source points are $P(r, \phi, z)$ and $Q(a, \phi', 0)$, respectively, with $d\vec{l}' = a\, d\phi'\hat{\phi}'$ and $\phi_1 \le \phi' \le \phi_2$, [10]. For this configuration, the cross product $d\vec{l}' \times (\vec{R} - \vec{R}')$ of (1) is

$$a\phi'\hat{\phi}' \times [(r\cos\phi - a\cos\phi')\hat{i} + (r\sin\phi - a\sin\phi')\hat{j} + z\hat{k}]. \tag{6}$$

As $\hat{\phi}' = -\sin\phi'\hat{i} + \cos\phi'\hat{j}$, the Cartesian version of this cross product is

$$[z\cos\phi'\ \hat{i} + z\sin\phi'\ \hat{j} + (a - r\cos(\phi - \phi'))\ \hat{k}]\ a\ d\phi' \tag{7}$$

$\vec{H}$ in (1) for this case becomes

$$\vec{H} = a\int_{\phi_1}^{\phi_2} d\phi' D^{-3} \begin{cases} z\cos\phi' \\ z\sin\phi' \\ a - r\cos(\phi - \phi') \end{cases} \tag{8}$$

where $D^2 = a^2 + r^2 + z^2 - 2ar\cos(\phi - \phi')$.

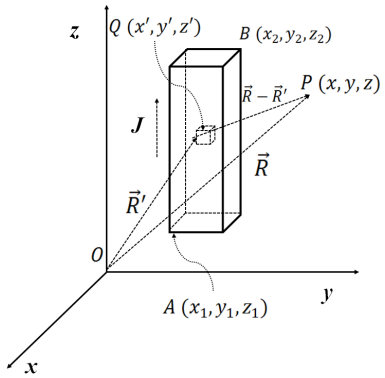

Fig. 3. Configuration of a straight rectangular cross-sectional slab.

C. Rectangular Cross-Sectional Slab

Fig. 3 shows the orientation of the rectangular cross-sectional slab for which we derive the formula.

The slab is kept parallel to the Z-axis with cross section $(x_2 - x_1) \times (y_2 - y_1)$ and height $(z_2 - z_1)$. The space and source points are $P(x, y, z)$ and $Q(x', y', z')$, respectively, with $d\vec{l}' = dz'\hat{k}$, $ds' = dx'dy'$, and $i_1 \le i' \le i_2, i = x, y, z$ [9]. For this configuration, the cross product $d\vec{l}' \times (\vec{R} - \vec{R}')$ of (2) is

$$dz'\hat{k} \times [(x - x')\hat{i} + (y - y')\hat{j} + (z - z')\hat{k}] = [v\hat{i} - u\hat{j}]\, dw \tag{9}$$

where $u = x - x'$, $v = y - y'$ and $w = z - z'$.

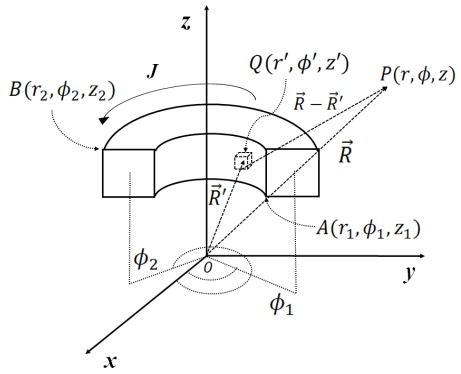

Fig. 4. Configuration of a circular arc of rectangular cross section.

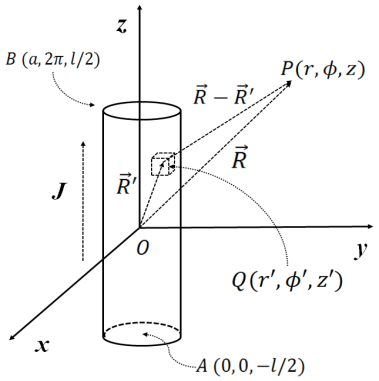

Fig. 5. Configuration of a cylindrical wire.

$\vec{H}$ in (2) for this case becomes

$$\vec{H} = \int_{u_1}^{u_2}\int_{v_1}^{v_2}\int_{w_1}^{w_2} \frac{du\ dv\ dw}{(u^2+v^2+w^2)^{\frac{3}{2}}} \begin{cases} v \\ -u \\ 0. \end{cases}$$

On integrating and substituting the limits

$$\vec{H} = \sum_{i,j,k=1}^{2} (-1)^{i+j+k} \begin{cases} \beth(u_i, v_j, w_k) \\ -\beth(v_j, u_i, w_k) \\ 0 \end{cases} \tag{10}$$

where

$$\beth(u_i, v_j, w_k) = v_j \tan^{-1}\left(\frac{u_i}{v_j}\cdot\frac{w_k}{\sqrt{u_i^2+v_j^2+w_k^2}}\right) - w_k \sinh^{-1}\left(\frac{u_i}{\sqrt{w_k^2+v_j^2}}\right) - u_i \sinh^{-1}\left(\frac{w_k}{\sqrt{u_i^2+v_j^2}}\right)$$

and $u_i = x - x_i, v_j = y - y_j$, and $w_k = z - z_k$.

D. Circular Arc of Rectangular Cross Section

Fig. 4 shows the orientation of the circular arc of rectangular cross section for which we derive the formula.

The circular arc is kept such that its axis coincides the Z-axis, the cross section is $(r_2 - r_1) \times (z_2 - z_1)$, and the azimuthal length is $(\phi_2 - \phi_1)$. The space and source points are $P(r, \phi, z)$ and $Q(r', \phi', z')$, respectively, with $d\vec{l}' = r' d\phi' \hat{\phi}'$, $ds' = dr'dz'$, and $i_1 \le i' \le i_2, i = r, \phi, z$ [11]. For this configuration, the cross product $d\vec{l}' \times (\vec{R} - \vec{R}')$ of (2) is

$$[(z-z')\cos\phi'\ \hat{i} + (z-z')\sin\phi'\ \hat{j} + (r'-r\cos(\phi-\phi'))\hat{k}]r'\ d\phi'. \tag{11}$$

Therefore, $\vec{H}$ in (2) for this case becomes

$$\vec{H} = \int_{r_1}^{r_2}\int_{\phi_1}^{\phi_2}\int_{z_1}^{z_2} dr'd\phi'dz'\ r'D^{-3} \begin{cases} (z-z')\cos\phi' \\ (z-z')\sin\phi' \\ r' - r\cos(\phi-\phi') \end{cases} \tag{12}$$

where $D^2 = r^2 + r'^2 + (z-z')^2 + 2rr'\cos(\phi-\phi')$.

E. Cylindrical Wire

Fig. 5 shows the orientation of the cylindrical wire for which we derive the formula.

The cylindrical wire is kept on the Z-axis, has a radius a and a height l. The space and source points are $P(r, \phi, z)$ and $Q(r', \phi', z')$, respectively, with $d\vec{l}' = dz'\hat{k}$, $ds' = r'dr'd\phi'$, and $0 \le r' \le a, \phi_1 \le \phi' \le \phi_2$ and $-l/2 \le z' \le l/2$. For this configuration, the cross product $d\vec{l}' \times (\vec{R} - \vec{R}')$ of (2) is

$$dz'\ \hat{k} \times [(r\cos\phi - r'\cos\phi')\ \hat{i} + (r\sin\phi - r'\sin\phi')\hat{j} + (z-z')\hat{k}]. \tag{13}$$

This simplifies to

$$[(r'\sin\phi' - r\sin\phi)\hat{i} + (r\cos\phi - r'\cos\phi')\hat{j}]\ dz'. \tag{14}$$

Therefore, $\vec{H}$ in (2) for this case becomes

$$\vec{H} = \int_0^a\int_0^{2\pi}\int_{-l/2}^{l/2} dr'd\phi'dz'\ r'D^{-3} \begin{cases} r'\sin\phi' - r\sin\phi \\ r\cos\phi - r'\cos\phi' \\ 0 \end{cases} \tag{15}$$

where $D^2 = r^2 + r'^2 + (z-z')^2 + 2rr'\cos(\phi-\phi')$.

The formulae for the magnetic field were derived in Cartesian form, that is, B_x, B_y, and B_z. The fully analytical form of the magnetic field in the case of the straight filament and the slab were used to save the computational time, whereas, for the other three elements, the complete analytical derivations are not possible as they involve elliptic integrals. Simpson's rule was employed here to get the final $\vec{B}$.

III. Magnetic Field Due to an Arbitrary Orientation of Electromagnet Elements

The magnetic field formulae for a single fixed configuration, where the rotation of the electromagnets about all the three axes is zero, were discussed in Section II. In most of the cases, the rotation is non zero. The best way to handle these axes rotations is by using an xyz-Euler rotation matrix, $\mathbf{R}$ [12]. The transformations 1 and 2 were defined using the rotation matrix $\mathbf{R}$. Then, the magnetic field calculations for the arbitrary orientation of electromagnets were carried out.

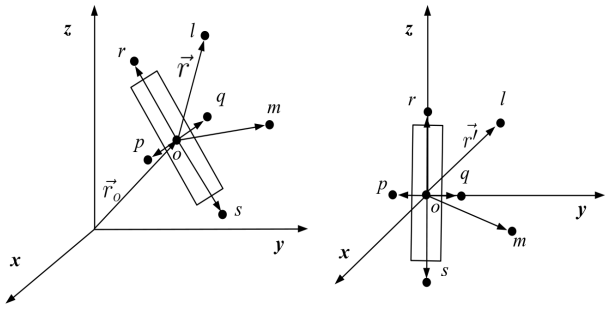

Fig. 6. (a) Arbitrary frame. (b) Specific configuration.

A. Transformation 1: Arbitrary to the Specific Orientation

An electromagnet with Euler rotation $\mathbf{R}$ and center $(\vec{r}_o)$ in the laboratory frame is shown in Fig. 6(a). The transformation to the specific configuration of the electromagnet for n space points is done as follows.

1) Construct the $(3 \times n)$ matrix $\tilde{r}$, where ith column of $\tilde{r}$ denotes the coordinate of ith space point.
2) Subtract $\tilde{r}_o$ from $\tilde{r}$ to coincide the center of the electromagnet with the origin, where $\tilde{r}_o$ is n times repetition of $\vec{r}_o$.
3) Apply $\mathbf{R}^{-1}$ to $\tilde{r} - \tilde{r}_o$. This operation coincides the electromagnet's axis with the Z-axis.

This procedure gives the new coordinates $(\tilde{r'})$ of the space points, which is related to the original coordinates $(\tilde{r})$ as

$$\tilde{r'} = \mathbf{R}^{-1} \cdot (\tilde{r} - \tilde{r}_o). \tag{16}$$

Fig. 6(b) shows the transformed space in which the electromagnets and the space points are brought to the fixed configuration as detailed in Section II and the magnetic fields $(\tilde{B'})$ are calculated using the derived formulae.

B. Transformation 2: Specific to Arbitrary Orientation

After calculating the magnetic fields, the transformation back to the original configuration of the electromagnets was done as

$$\tilde{r} = \mathbf{R} \cdot \tilde{r'} + \tilde{r}_o \tag{17}$$

$$\tilde{B} = \mathbf{R} \cdot \tilde{B'} \tag{18}$$

where ith column of $\tilde{B}$ is the magnetic field for the corresponding space point (ith column of $\tilde{r}$). The second equation is obvious from the fact that the magnetic field is only a function of the distance between the electromagnet and the space point. Since the axes have been rotated, the Euler rotation matrix can be applied to establish a relationship between the transformed and real fields.

IV. Flow of CAE v1.1 Code

The code CAE v1.1 is written in Python 3.6 language owing to its easy matrix handling, vast libraries and free availability for the popular operating systems. CAE v1.1 is a union of the main code CAE.py and the submodules: 1) Inputs.py and 2) Magnet modules.

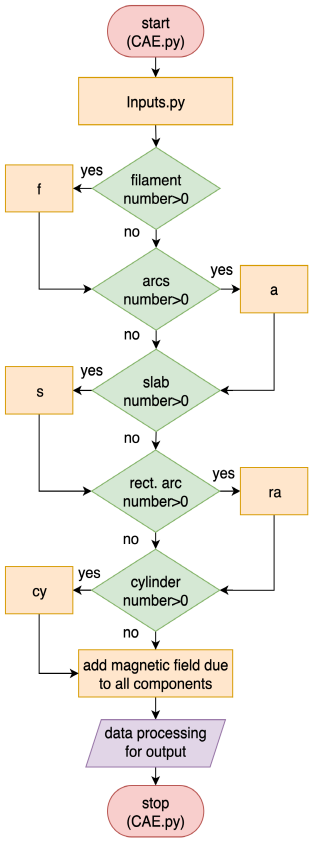

Fig. 7. Flowchart for CAE.py.

A. Structure of the Main Code: CAE.py

Fig. 7 illustrates the flowchart of the main code, CAE.py. This code calls all the submodules.

The module Inputs.py validates the input data. "Magnet modules" only calculate the magnetic fields due to individual electromagnet elements. In most of the applications, more than one electromagnet is used to generate the desired shapes and values of the magnetic field. As the magnetic fields are additive, that is, the resultant field at a space point is the vector sum of fields due to individual electromagnets, CAE.py does the final vector addition and process the data to output the results.

B. Details of Input Files

1) Input Files: This code requires two input files in the popular Microsoft Excel format (2013 or 97-2003), named, CAE_1.xlsx and CAE_2.xlsx. The SI unit system is chosen for the inputs except for the angles (rather than radians, degrees are used to avoid fractions).

The user can enter the data regarding five types of electromagnet elements in the CAE_1.xlsx. These data cover the dimensions, the locations in space (i.e., centers and Euler angles), and the currents (or the current densities) as depicted in the snippet Fig. 8.

In CAE_2.xlsx, the user has to enter the data regarding the space points where the magnetic field is required. To adjust the permeability of space, "permeability" option is incorporated. Various logical plotting options viz. "3-D plots," "contour

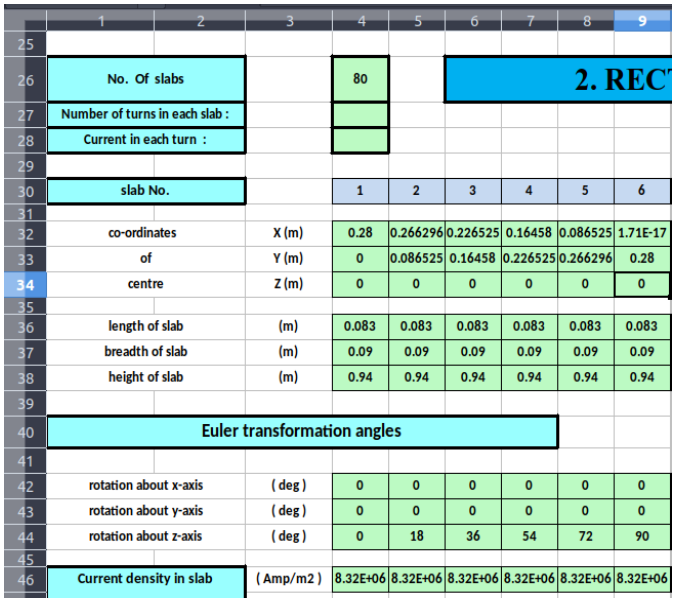

No. Of slabs			80			2. REC		
Number of turns in each slab :								
Current in each turn :								
slab No.			1	2	3	4	5	6
co-ordinates	X (m)		0.28	0.266296	0.226525	0.16458	0.086525	1.71E-17
of	Y (m)		0	0.086525	0.16458	0.226525	0.266296	0.28
centre	Z (m)		0	0	0	0	0	0
length of slab	(m)		0.083	0.083	0.083	0.083	0.083	0.083
breadth of slab	(m)		0.09	0.09	0.09	0.09	0.09	0.09
height of slab	(m)		0.94	0.94	0.94	0.94	0.94	0.94
Euler transformation angles								
rotation about x-axis	(deg)		0	0	0	0	0	0
rotation about y-axis	(deg)		0	0	0	0	0	0
rotation about z-axis	(deg)		0	18	36	54	72	90
Current density in slab	(Amp/m2)		8.32E+06	8.32E+06	8.32E+06	8.32E+06	8.32E+06	8.32E+06

Fig. 8. Input entry file snippet of CAE_1.xlsx.

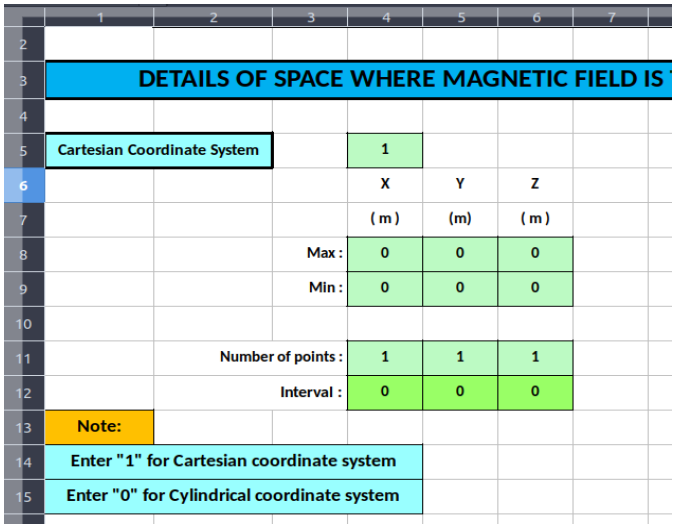

DETAILS OF SPACE WHERE MAGNETIC FIELD IS				
Cartesian Coordinate System		1		
		X	Y	Z
		(m)	(m)	(m)
	Max :	0	0	0
	Min :	0	0	0
	Number of points :	1	1	1
	Interval :	0	0	0
Note:				
Enter "1" for Cartesian coordinate system				
Enter "0" for Cylindrical coordinate system				

Fig. 9. Input entry file snippet-1 of CAE_2.xlsx.

plots," and "current direction" can be entered as depicted in the snippet Figs. 9 and 10.

2) CAEB v1.1: In most of the electromagnetic systems, the coils are arranged in a symmetric manner, for example, Tokamak. The CAEB v1.1—CAE Builder code takes advantage of the symmetry and minimizes the complexities of generating the input Excel files for the coils. The CAEB v1.1 reads the CAE_1.xlsx file that has inputs for one coil, number of coils in a system and generates an output file, Builder.xlsx with the data of all the coils.

C. Details of Magnet Modules

"Magnet modules" is the most important part of CAE v1.1. This part is made up of five modules: 1) the straight filament; 2) the circular filament; 3) the straight slab; 4) the circular arc of rectangular cross section; and 5) the cylindrical wire.

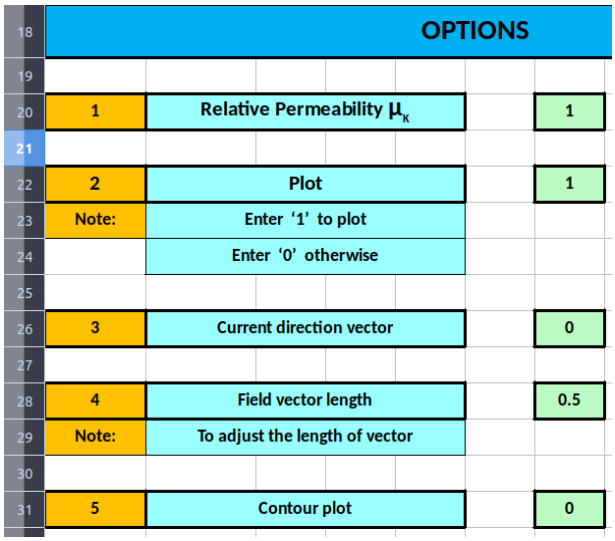

OPTIONS		
1	Relative Permeability μ_K	1
2	Plot	1
Note:	Enter '1' to plot	
	Enter '0' otherwise	
3	Current direction vector	0
4	Field vector length	0.5
Note:	To adjust the length of vector	
5	Contour plot	0

Fig. 10. Input entry file snippet-2 of CAE_2.xlsx.

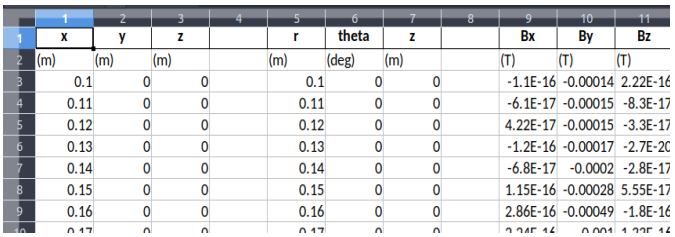

x	y	z		r	theta	z		Bx	By	Bz
(m)	(m)	(m)		(m)	(deg)	(m)		(T)	(T)	(T)
0.1	0	0		0.1	0	0		-1.1E-16	-0.00014	2.22E-16
0.11	0	0		0.11	0	0		-6.1E-17	-0.00015	-8.3E-17
0.12	0	0		0.12	0	0		4.22E-17	-0.00015	-3.3E-17
0.13	0	0		0.13	0	0		-1.2E-16	-0.00017	-2.7E-20
0.14	0	0		0.14	0	0		-6.8E-17	-0.0002	-2.8E-17
0.15	0	0		0.15	0	0		1.15E-16	-0.00028	5.55E-17
0.16	0	0		0.16	0	0		2.86E-16	-0.00049	-1.8E-16

Fig. 11. Output file snippet of MAG_DATA.xlsx.

These modules are written as individual functions to calculate the magnetic field using the derived mathematical equations whose details are given in Section II.

V. Output

CAE v1.1 generates three kinds of output: 1) Microsoft Excel 2013 MAG_DATA.xlsx file; 2) contour plots; and 3) 3-D plots.

A. Output File

The code generates MAG_DATA.xlsx, the output file that contains the space data points and the corresponding values of the magnetic field in both the Cartesian and cylindrical frames useful for further analysis as shown in Fig. 11.

B. Contour Plots

For ease of visualization, the code generates two contour plots (filled and line) of $|\vec{B}|$ where the space data points vary in a plane and are constant along the perpendicular axis. Fig. 12 shows the line contour of ADITYA-U tokamak.

C. 3-D Plots

As an electromagnet is made up of many elements whose data contains numerous values, the correctness of data entered can only be ensured by the visual outputs of the code. Hence, this code outputs 3-D plots of the electromagnets with the magnetic field vectors to visualize the system. For the straight filament and the slab, one additional option of current direction was also incorporated.

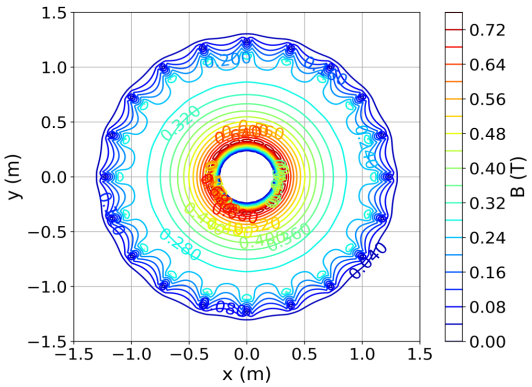

Fig. 12. Line contour of ADITYA-U tokamak with current density $J = 8.32e6$ A/m^2 in $z = 0$ plane.

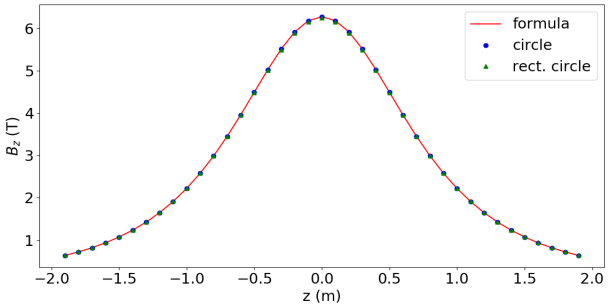

Fig. 13. Magnetic field along z-axis due to circular coil with a =1 m and current $I = 1e7$ A.

VI. Verification of the Code

The successful verification of CAE v1.1 is done with: 1) two standard examples and 2) existing EFFI code.

A. With Standard Examples

The verification of the code was done with the two popular standard examples: 1) the circular ring having a radius a and 2) Helmholtz coils with a radius a. The magnetic field on the axis was calculated by considering the two options in the code—the circular filament and the circular arc of rectangular cross section (0.01×0.01 m^2) with the formulae

$$B_{\text{circle}} = \frac{\mu_0 I}{2a}(\gamma^2 + 1)^{-\frac{3}{2}} \tag{19}$$

$$B_{\text{Helmholtz}} = \frac{\mu_0 I}{2a}\sum_{i=1}^{2}\left(\gamma^2 + (-1)^i\gamma + \frac{5}{4}\right)^{-\frac{3}{2}} \tag{20}$$

where $\gamma = z/a$.

Fig. 13 clearly shows a good agreement between: 1) the formula for a circular coil and the code for a circular filament ($< 0.013\%$) and 2) the formula for a circular coil and the code for a circular arc of the rectangular cross section of small dimensions ($< 0.393\%$).

Fig. 14 clearly shows a good agreement between: 1) the formula for Helmholtz coils and the code for circular filaments ($< 0.013\%$) and 2) the formula for Helmholtz coils and the code for circular arcs of the rectangular cross section of small dimension ($< 0.362\%$).

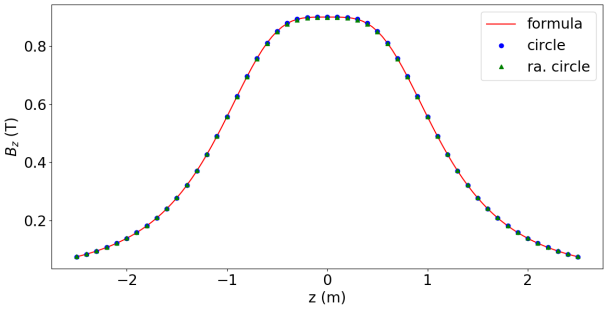

Fig. 14. Magnetic field along z-axis due to Helmholtz arrangement of coils with a =1 m and current $I = 1e6$ A.

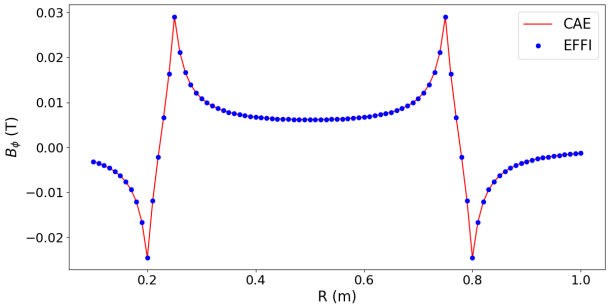

Fig. 15. Magnetic field across one TF coil of BETA machine along $z = 0$, $\phi = 0°$ and $J = 2e6$ A/m^2.

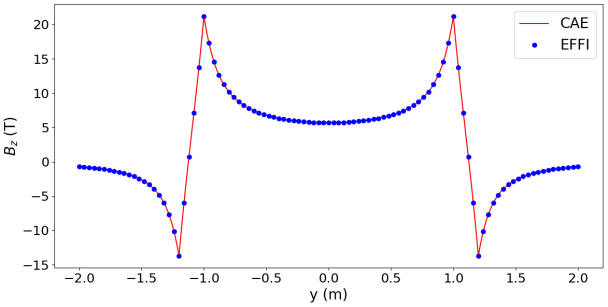

Fig. 16. Circular coil with rectangular cross section in $z = 0, xy$ plane, $I = 1e7$ A, cross section 0.2×0.2 m^2.

B. With EFFI Code

The verification of CAE with EFFI was done by calculating the magnetic field: 1) along $z = 0$ and $\phi = 0$ line for a single TF-coil of the BETA as in Fig. 15 and 2) along $z = 0$ and $x = 0$ line for a circular coil of rectangular cross section as in Fig. 16.

Figs. 15 and 16 clearly show fair agreement of results ($< 0.099\%$ and $< 0.528\%$, respectively) between CAE v1.1 and EFFI (by considering the step size as 0.001 in the simps function of SciPy library in Python 3.6).

VII. Results

A. BETA Machine

The CAE v1.1 was used to generate the TF coils system of BETA machine using one element: straight slab, as shown in Fig. 17.

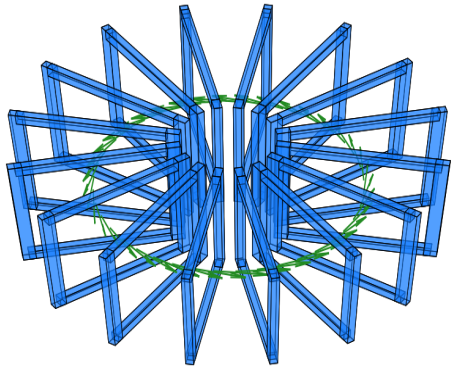

Fig. 17. BETA machine with all 16 TF coils, major radius of 0.45 m and minor radius of 0.15 m.

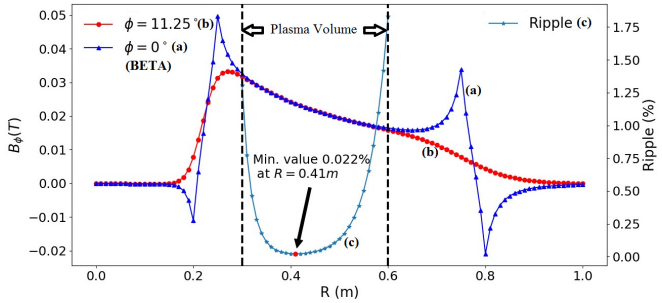

Fig. 18. B_ϕ versus R plots at (a) TF-coil location $\phi = 0°$, (b) in between two TF-coils $\phi = 11.25°$, and (c) ripple % for BETA.

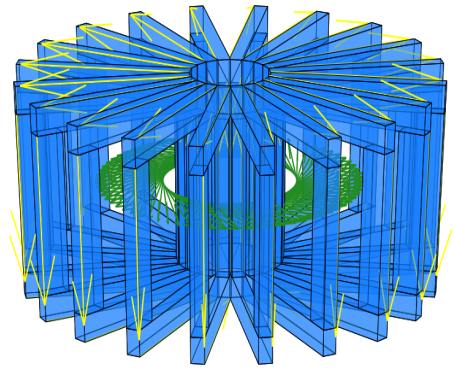

Fig. 19. ADITYA-U tokamak with all 20 TF coils, major radius of 0.75 m and minor radius of 0.25 m.

The plots of the toroidal magnetic field (B_ϕ) versus radius (R) at (a) the TF-coil location, (b) between the two TF-coils, and (c) the ripple % for this electromagnet system is shown in Fig. 18.

B. ADITYA-U

The CAE v1.1 was used to generate the TF coils system of ADITYA-U [1] using one component: straight slab, as shown in Fig. 19.

The plots of the toroidal magnetic field (B_ϕ) versus radius (R) at (a) the TF-coil location, (b) between the two TF-coils, and (c) the ripple % for this system is shown in Fig. 20.

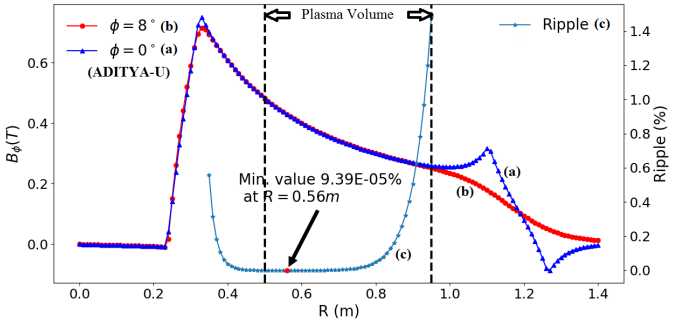

Fig. 20. B_ϕ versus R plots at (a) TF-coil location $\phi = 0°$, (b) in between two TF-coils $\phi = 8°$, and (c) ripple% for ADITYA-U.

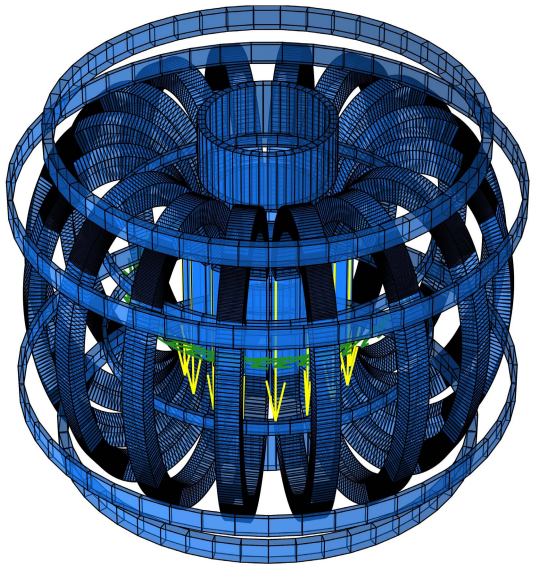

Fig. 21. SST-1 tokamak with all 16 TF and 12 PF coils, major radius of 1.1 m and minor radius of 0.2 m.

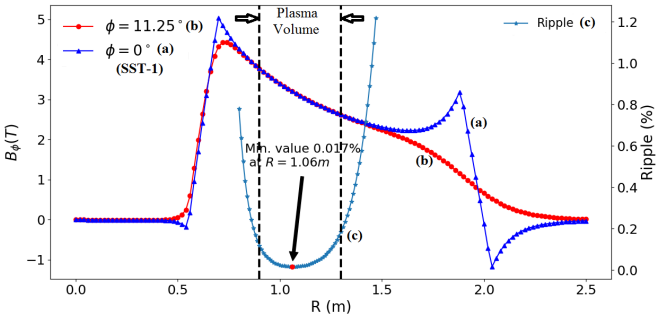

Fig. 22. B_ϕ versus R plots at (a) TF-coil location $\phi = 0°$, (b) in between two TF-coils $\phi = 11.25°$, and (c) ripple % for SST-1.

C. SST-1

The CAE v1.1 was used to generate all the TF and PF coils of SST-1 [3] using the combination of two elements: straight and circular bars, as shown in Fig. 21.

The plots of the toroidal magnetic field (B_ϕ) versus radius (R) at (a) the TF-coil location, (b) between the two TF-coils, and (c) the ripple % is shown in Fig. 22.

Figs. 18, 20, and 22 clearly show that the ripple $= (B_{\phi\max} - B_{\phi\min}/B_{\phi\max} + B_{\phi\min}) \times 100\%$ for these systems is in good agreement with "$< 2\%$ within plasma volume," an important design parameter.

VIII. Conclusion

The formulas for the magnetic field components due to the current in: 1) the straight filament; 2) the circular filament; 3) the rectangular cross-sectional slab; 4) the circular arc of rectangular cross section; and 5) the cylindrical wire conductors were successfully derived from the fundamental Biot–Savart law analytically and using Simpson's method (numerically, wherever required).

The ease of usage, when compared to other codes like EFFI, was implemented by using the MS Excel file format for the two input files required by the code. The analysis of the output data was also made easy by using: 1) the MS Excel output file format only and the data in both the Cartesian and cylindrical frames; 2) the contours; 3) the visuals of electromagnets; and 4) the plots of magnetic field versus R and the Ripple (depending on the options chosen).

The CAE v1.1 written in the free programming language Python 3.6 was successfully tested without any modifications both on the Windows 10 and the Ubuntu 18.04 operating systems. The code is also compatible with both the MS Excel formats—2013 (present) and 97–2003 (previous) of input-output files that makes this a better choice over other existing codes. This code CAE v1.1 is also successfully verified with: 1) the standard examples and 2) the available Linux based ForTran-EFFI. The code was successfully used for BETA, ADITYA-U, and SST-1 of IPR by calculating: 1) the toroidal magnetic fields at the TF-coil center and between the two TF coils and 2) Ripple % within the plasma volume.

The modules viz.: 1) error-field calculations; 2) optimization of TF coils; 3) magnetic force and inductance; and 4) electric fields and also usage of this code CAE v1.1 for charged particle motion are planned for the extension of this work in the future.

References

[1] J. Ghosh *et al.*, "Upgrade of ADITYA Tokamak with limiter configuration to ADITYA upgrade tokamak with divertor configuration," in *Proc. 26th IAEA Fusion Energy Conf.*, Kyoto, Japan, Oct. 2016, p. 417.

[2] D. H. Sadharakiya, R. L. Tanna, and J. Ghosh, "The refurbishment of damaged toroidal magnetic field coils for ADITYA upgrade," in *Proc. 10th Asia Plasma Fusion Assoc. Conf. (APFA)*, Gandhinagar, India, Dec. 2015.

[3] Y. C. Saxena, "Manufacturing of magnets for SST-1 Tokamak," in *Proc. 3rd IAEA TCM Oper. Magn. Fusion Devices Conf.*, Mar. 2013.

[4] S. J. Sackett, "EFFI: A code for calculating the electromagnetic field, force, and inductance in coil systems of arbitrary geometry," LLL, Univ. California, Oakland, CA, USA, Tech. Rep. UCRL-52402, Mar. 1978.

[5] D. V. Anderson, J. Breazeal, C. H. Finan, and B. M. Johnston, "ABCXYZ: Vector potential (A) and magnetic field (B) code (C) for Cartesian (XYZ) geometry using general current elements," LLL, Univ. California, Oakland, CA, USA, Tech. Rep. UCRL-52029, Sep. 1976.

[6] W. A. Perkins and J. C. Brown, "MAFCO—A magnetic field code for handling general current elements in three dimensions," *J. Appl. Phys.*, vol. 35, no. 11, p. 3337, Apr. 1964.

[7] B. Manes, "TOKEF: A tokamak input generator for EFFI," ITEP, Berlin, Germany, Tech. Rep. KfK 3854, Dec. 1984.

[8] D. R. Prajapati and G. R. Babu, "A code for magnetic field due to arbitrary electromagnets (CAE v1.0)," IPR, Gandhinagar, India, Tech. Rep. IPR/TR-468/2018, Feb. 2018.

[9] M. Kundu and S. P. Deshpande, "Analytical derivation of magnetic field and vector potential due to different current carrying conducting geometries," IPR, Gandhinagar, India, Tech. Rep. IPR\TR-97\2003, Jul. 2003.

[10] L. K. Urankar, "Vector potential and magnetic field of current-carrying finite arc segment in analytical form, Part I: Filament approximation," *IEEE Trans. Magn.*, vol. MAG-16, no. 5, pp. 1283–1288, Sep. 1980.

[11] L. K. Urankar, "Vector potential and magnetic field of current-carrying finite arc segment in analytical form, Part III: Exact computation for rectangular cross section," *IEEE Trans. Magn.*, vol. MAG-18, pp. 1860–1867, Nov. 1982.

[12] G. G. Slabaugh, "Computing Euler angles from a rotation matrix," Huawei Technol. Res. Develop., London, U.K., Tech. Rep., Aug. 2000, pp. 39–63.